ELSEVIER

Spectrochimica Acta Part B 55 (2000) 1465–1479

SPECTROCHIMICA ACTA PART B

www.elsevier.nl/locate/sab

Comparison of calculated and measured optical emission intensities in a direct current argon–copper glow discharge

Annemie Bogaerts[a,*], Zoltan Donko[b], Kinga Kutasi[b], Gregor Bano[b], Nuno Pinhao[c], Mario Pinheiro[d]

[a] *Department of Chemistry, University of Antwerp (UIA), Universiteitsplein 1, B-2610 Wilrijk-Antwerp, Belgium*
[b] *Research Institute for Solid State Physics and Optics, P.O. Box 49, H-1525 Budapest, Hungary*
[c] *Physics Department, Instituto Tecnologico e Nuclear, Estrada Nacional 10, 2685 Sacavém, Portugal*
[d] *Physics Department, Instituto Superior Técnico, Av. Rovisco Pais, 1049-001 Lisboa, Portugal*

Received 24 March 2000; accepted 16 June 2000

Abstract

Based on a collisional–radiative model for argon atoms and copper atoms and (Cu^+) ions, which was developed as a part of a comprehensive simulation network, optical emission intensities have been calculated for argon and copper lines in a direct current argon glow discharge with copper cathode. Comparison with experimental data has been made, both with respect to the optical emission spectra and to some selected emission lines as a function of axial position. From this study, information can be obtained about the importance of various plasma processes, like electron, fast ion and fast atom impact excitation, and reabsorption of resonant radiation.

Keywords: Collisional–radiative model; Argon; Copper; Optical emission

1. Introduction

Glow discharges are used in a growing number of application fields, e.g. in the semiconductor industry for etching and deposition of layers, in materials technology for the deposition of hard coatings, as lasers, light sources, plasma display panels, etc. Moreover, they also find application in analytical chemistry, for the spectrochemical analysis of (mainly) solid materials [1,2]. For the latter application, the material to be analyzed is used as the cathode of the glow discharge, which is sputter-bombarded by plasma species. The

* Corresponding author. Tel.: +32-3820-2364; fax: +32-3820-2376.
E-mail address: bogaerts@uia.ua.ac.be (A. Bogaerts).

0584-8547/00/$ - see front matter
PII: S0584-8547(00)00253-6

sputtered (analytically important) cathode-atoms arrive in the plasma, where they can be ionized or excited. The resulting ions can be measured with a mass spectrometer whereas the photons created by excitation and subsequent radiative decay, can be detected with an optical emission spectrometer.

We try to obtain a better insight into the optical emission spectral intensities, which is not only relevant to analytical glow discharge spectrometry, but also to optical spectrometric plasma diagnostic techniques. Therefore, a model has recently been developed to calculate the level populations of various excited levels of argon and copper species [3,4], and from this, the optical emission intensities can be derived [5,6].

In the literature, a number of papers have reported experimental optical emission intensities [7–13] and the occurrence of various processes, like cascading, stepwise excitation, etc., have been explained by some simple models [14–16]. Especially the spatial distribution of the emission lines is of great interest, to achieve better insight in the role of various excitation processes [7–10]. The lines which are most often studied, are the ArI 750.3 nm and the ArI 811.5 nm lines, because they are characterized by high intensities and they reflect some typical excitation processes [7–12,14].

In the present paper, we want to make a detailed comparison, at exactly the same discharge conditions and cell geometry, between calculated and experimental optical emission intensities. Some of the experimental results have already been published in [10] without detailed self-consistent models. The comparison will be performed for a range of operating conditions in a direct current (d.c.) argon glow discharge with a copper cathode. Special attention will be paid to the spatial behavior of some selected emission lines, in order to obtain information about various excitation processes in the plasma.

2. Short description of the model

In previous work, we have developed a comprehensive modeling network, consisting of Monte Carlo, fluid and collisional–radiative models for various plasma species: electrons, argon atoms, argon (Ar^+, Ar^{2+} and Ar_2^+) ions, argon atoms in various excited levels, sputtered copper atoms and the corresponding Cu^+ ions, both in the ground state and also in various excited levels. Typical results of the modeling network, include among others the electric field and potential distribution, densities, fluxes and energies of the electrons, ions and neutrals, and information about collision processes in the plasma [17]. More detailed information can be found in work by Bogaerts [17]. Only the models relevant to the present work, i.e. the collisional–radiative models, will be described in some more detail.

A collisional–radiative model is used to calculate the level populations of various excited levels. It consists of a set of balance equations (one for each level) with different production and loss terms. The production and loss processes are all of collisional or radiative nature (e.g. electron impact excitation or radiative decay), hence the name of this type of models.

The collisional–radiative model we developed for the argon atoms takes into account 65 argon levels [3]. Some of these levels (like the four 4s levels) are considered separately, but most levels are a group of individual levels with similar excitation energy and quantum numbers. The collisional and radiative processes taken into account are radiative decay, electron, fast argon ion and fast and thermal argon atom impact ionization, excitation and de-excitation between all the levels, electron-ion radiative recombination, electron-ion three-body recombination where the third body is an electron or an argon gas atom (although it should be mentioned that electron-ion recombination is found to be more or less negligible at the conditions under study, except at the cell walls), and Hornbeck–Molnar associative ionization (for levels with excitation energy above 14.71 eV). Some additional processes are incorporated for the 4s levels, i.e. Penning ionization of sputtered atoms, two- and three-body collisions with argon ground state atoms, collisions between two 4s atoms, and diffusion and subsequent de-excitation at the walls. More information about this model and about the relative importance of the

various processes can be found in work by Bogaerts et al. [3]. We have, however, slightly modified the collisional–radiative model of Bogaerts et al. [3], by including a radiation escape factor dependent on radial position [18], to account for differences in radiation absorption at different positions from the central axis.

A similar collisional–radiative model was constructed for the copper atoms, together with a model for the copper ions [4]. This model includes a set of balanced equations for eight copper atomic levels, seven Cu^+ ionic levels, as well as for the Cu^{2+} ions. Some levels are individual levels and others are groups of levels, depending on their excitation energy and quantum numbers. The relevant processes are electron, argon and copper atom impact excitation and de-excitation between the various levels, as well as radiative decay between the levels, electron impact ionization and electron-ion three-body recombination. Moreover, Penning ionization with argon metastable atoms and asymmetric charge transfer with argon ions are taken into account as additional ionization processes. Further information is given in work by Bogaerts et al. [4].

As mentioned before, these collisional–radiative models are part of a comprehensive modeling network [17]. The only input parameters for the model network are discharge voltage, gas pressure and temperature, and the discharge geometry (see below), as well as the cross-sections for all collision processes. The output of the Monte Carlo and fluid models, such as the electron energy distribution function, electric field, electron and argon ion densities and reaction rates, are used to solve the collisional–radiative models.

Finally, the optical emission intensities for a given transition are calculated by multiplying the level populations of the excited levels with the Einstein transition probabilities for radiative decay. With our present model, the intensities of 605 argon atomic lines and 103 copper atomic and ionic lines could be calculated.

3. Experimental setup

The experimental setup is the same as in Donko et al. [10]. A direct current discharge was created between two flat disk copper electrodes with a diameter of 3.14 cm, at a distance of 4.5 cm from each other. The electrodes were confined in a metal tube at floating potential, with an internal diameter 0.07 cm larger than the electrode diameter. The spatial distribution of the light intensity in the discharge was scanned in the axial direction through a slit machined into the floating tube with 0.5 mm width. The background pressure of the vacuum system was $\sim 10^{-6}$ mbar, and the purity of the argon filling gas was 99.999%.

The light intensity distribution measurements were controlled by a PC. The discharge tube was mounted on a translator, equipped with a stepping motor under computer control. The discharge light was imaged onto the entrance slit of a 2-m monochromator with a 100-mm focal length quartz lens. A diaphragm of 5 mm diameter was placed in front of the lens to obtain a lateral spatial resolution of ~ 0.3 mm. For measurements in the ultraviolet and blue part of the spectrum, an EMI 6256S photomultiplier tube (PMT) was used, while an EMI 9558B PMT was applied for the near-infrared part of the spectrum. The signal of the PMT was sent to a HP54501A digitizing oscilloscope connected to the PC, using an IEEE488 interface. Finally, the PC also controlled the wavelength positioning of the monochromator when recording the spectral scans.

4. Results and discussion

4.1. Electrical characteristics of the discharge

The discharge conditions investigated in this work, both experimentally and in the model, i.e. the currents and current densities (left and right axis, respectively) as a function of voltage for different pressures, are illustrated in Fig. 1. In the model, the current is calculated self-consistently (i.e. as the sum of the microscopic fluxes of the charged plasma species) when the voltage, the gas pressure and temperature are given as input. Since we wanted to perform the calculations for exactly the same conditions of voltage, pressure and cur-

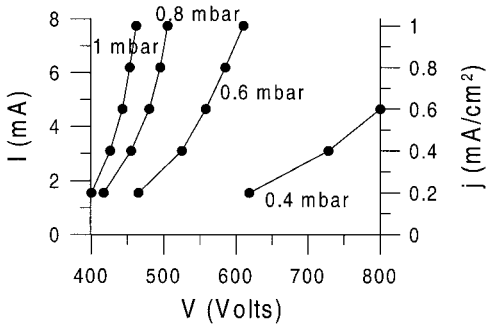

Fig. 1. Discharge conditions investigated in the present work, both experimentally and in the model.

rent as in the measurements, and since the exact value of the experimental gas temperature was not known, we have adapted the latter value in order to obtain similar currents as in the experiment, for the same voltage and pressure. The values of the gas temperature ranged hereby from 300 to 500 K, which is realistic for the conditions under investigation [19]. This shows that the model gives a satisfactory prediction of the electrical current at a given discharge voltage.

Fig. 2 presents the two-dimensional potential distribution at 1 mbar, 443 V and 4.65 mA (0.6 mA/cm^2). The potential is −443 V at the cathode and increases rapidly until zero at approximately 2–2.3 mm from the cathode (varying slightly in the radial direction). It becomes slightly positive (less than 10 V) in the remainder of the plasma. This potential distribution shows clearly the subdivision between the cathode dark space (CDS) and negative glow (NG). Indeed, we defined the thickness of the CDS as the position where the potential crosses the zero line (approx. 2–2.3 mm in this case; see thicker line). The potential changes rapidly in the CDS (giving rise to a high electric field), and it is slightly positive

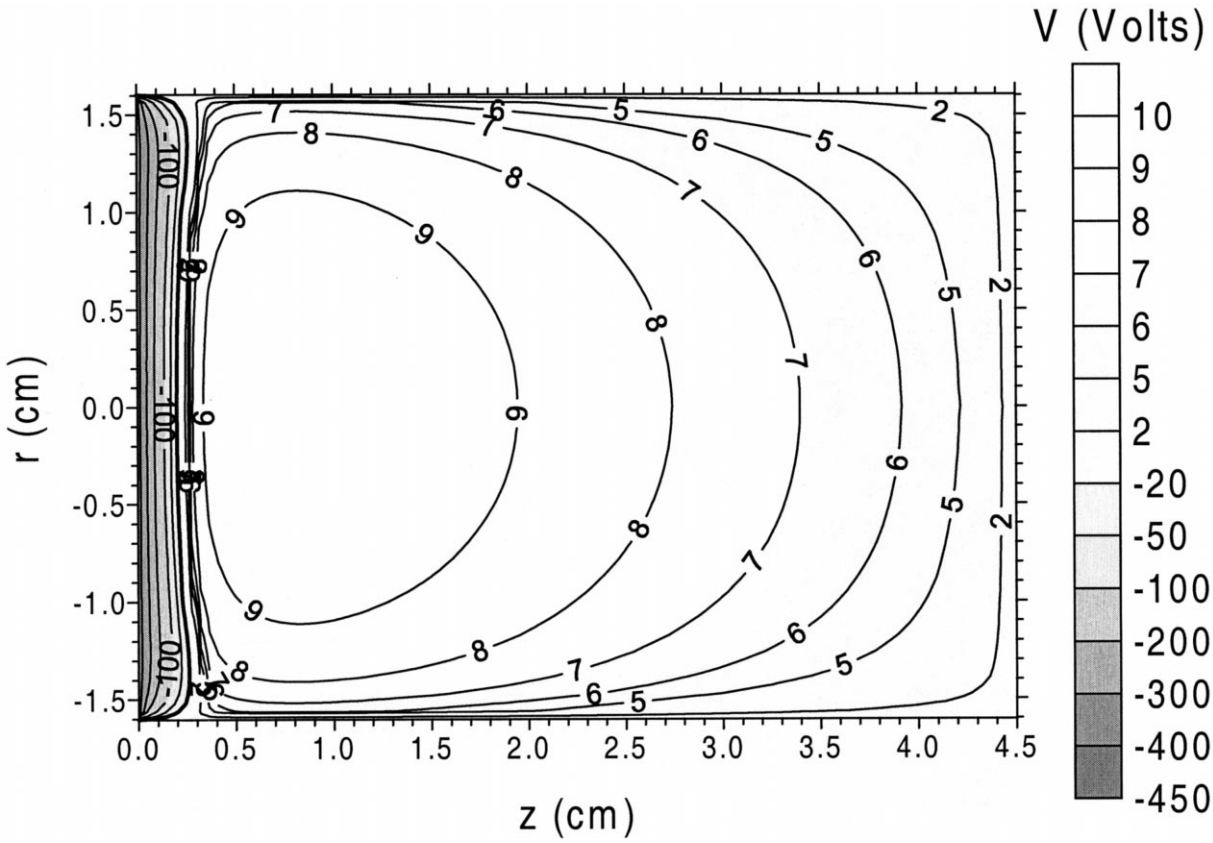

Fig. 2. Calculated two-dimensional potential distribution at 1 mbar, 443 V and 0.6 mA/cm^2.

and nearly constant in the NG (resulting in a low electric field). It is also clear that the glow discharge consists only of a CDS and an NG at the conditions under study. This picture should be kept in mind when explaining the calculated and measured optical emission intensities.

4.2. Optical emission spectrum

The calculated optical emission spectrum, consisting both of argon atomic lines, and copper atomic and ionic lines, is shown in Fig. 3, for the same conditions as in Fig. 2. Two different locations in the plasma are illustrated, i.e. (a) adjacent to the cathode (the so-called cathode glow, CG, this is the region in the CDS near the cathode which is rather bright, in contrast to the remaining of the CDS) and (b) at 0.23 cm from the cathode (i.e. in the beginning of the negative glow, NG). It is clear that at both locations the lines in the region of 700–1000 nm are most intense. These are the so-called ArI red lines, corresponding to 4p–4s transitions. Beside these lines, also some lines in the region of 400–440 nm are observed, both in the CG and in the beginning of the NG, as appears from the enlarged 200–700 nm region in Fig. 3a,b. These lines correspond to ArI 5p–4s transitions, and their intensities are lower than the 4p–4s lines by a factor of 500 in the CG, and by a factor of approximately 30 in the NG. In the CG nearly no other lines are visible in the spectrum, but in the NG, some ArI lines originating from higher excited levels are present in the region between 500 and 700 nm. Moreover, the enlarged part in Fig. 3b shows also the CuI resonant lines at 324.7 and 327.4 nm in the NG spectrum, as well as the CuII line at 224.7 nm, which results from selective asymmetric charge transfer population of a Cu^+ level [20].

Since the red lines are clearly dominant in the spectrum, we have zoomed in on the region between 680 and 820 nm, in order to compare the calculated intensities in this region with the experimental intensities. This comparison between the calculated and the measured spectra is presented in Fig. 4, for the same discharge conditions as in Fig. 3, and at the same two locations in the plasma, i.e. in the CG [(a) for the model and (b) for the experiment], and in the beginning of the NG [(c) for the model and (d) for the experiment]. Reasonable agreement could be reached between model and experiment, since the same lines are present in both spectra, with similar relative intensities. An exception was found for the ArI 811.53 nm and 750.38 nm lines in the NG. Indeed, the model predicts that the 811.53 nm line is more intense than the 750.38 nm line in the NG, whereas experimentally the opposite trend was observed. A possible reason might be that the upper level of the 811.53 nm line (i.e. the 4p $[5/2]_3$ level) is slightly overpopulated in the model (maybe too high values for the excitation cross-sections) or that the upper level of the 750.38 nm line (i.e. the 4p′ $[1/2]_0$ level) is somewhat underpopulated. Alternatively, the Einstein transition probabilities used in the model for the 811.53 nm and the 750.38 nm lines might be somewhat too high or too low, respectively. On the other hand, the experimental line intensities, especially in the high wavelength-range (such as for the 811.53 nm line), are also subject to some uncertainty (although probably not so high to completely explain the observed discrepancy), due to the relatively lower sensitivity of the PMT in this wavelength range.

It becomes also clear from Fig. 4a–d that some lines have high intensity in the CG and lower intensity in the NG [e.g. the ArI 811.53 nm line: calculated intensity (in a.u.) of 25 in the CG and of 10 in the NG, and measured intensity of 4 in the CG and of 2.5 in the NG], and that other lines exhibit the opposite trend [e.g. the ArI 750.38 nm line: calculated intensity of 1 in CG and of 3 in NG, and measured intensity of 1.2 in CG and of 5 in NG]. The reason for this is that these lines originate from different upper levels, and that different excitation processes are responsible for populating the upper levels at different locations in the plasma. Indeed, in the NG, electron impact excitation is generally the dominant excitation process for argon atomic levels, with a cross section reaching a maximum at approximately 20–30 eV for the 4p levels [21]. In the CG, however, two other processes, i.e. fast argon ion and atom impact excitation, can become quite important, especially at high voltages where the ions and

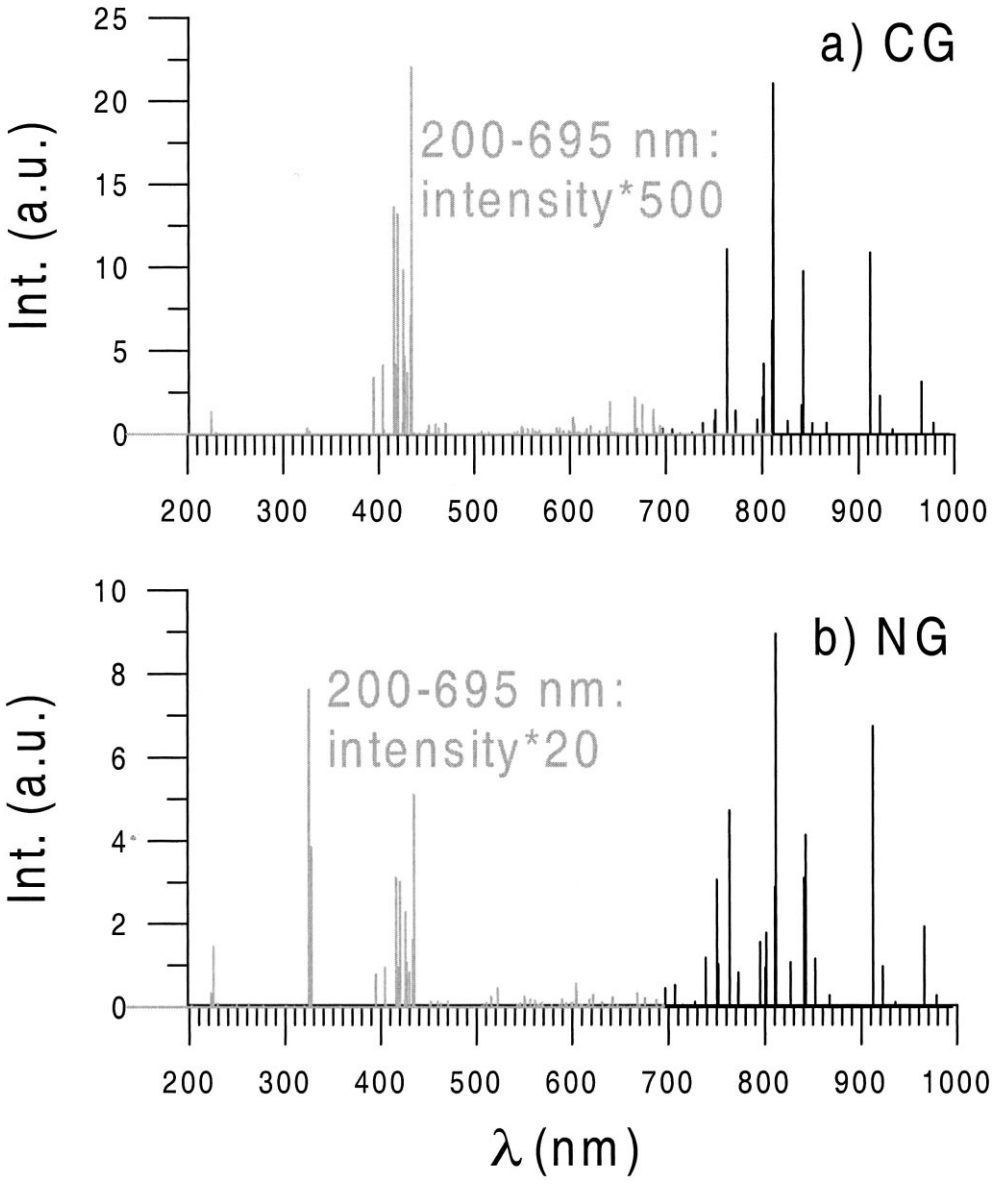

Fig. 3. Calculated optical emission spectra of argon atomic and copper atomic and ionic lines, in the CG (a) and in the beginning of the NG (b), at 1 mbar, 443 V and 0.6 mA/cm^2. The region of 200–700 nm is enlarged by a factor of 500 for (a) and 20 for (b).

atoms can reach high energies. Indeed, the cross-sections presented in [22] illustrate that these processes start to become important at energies of approximately 100 eV (for 811 nm emission). Since the ions and atoms reach the highest energy adjacent to the cathode, they cause only excitation in the region close enough to the cathode, which is, therefore, called the CG.

It is obvious, based on energy considerations, that all argon atomic levels can be populated by electron impact excitation at the discharge conditions under investigation (because the electrons have enough energy for excitation), but only the lowest levels (i.e. 4s and low 4p levels) can also be populated by fast argon ion and atom impact excitation. Indeed, the cross sections for ion and

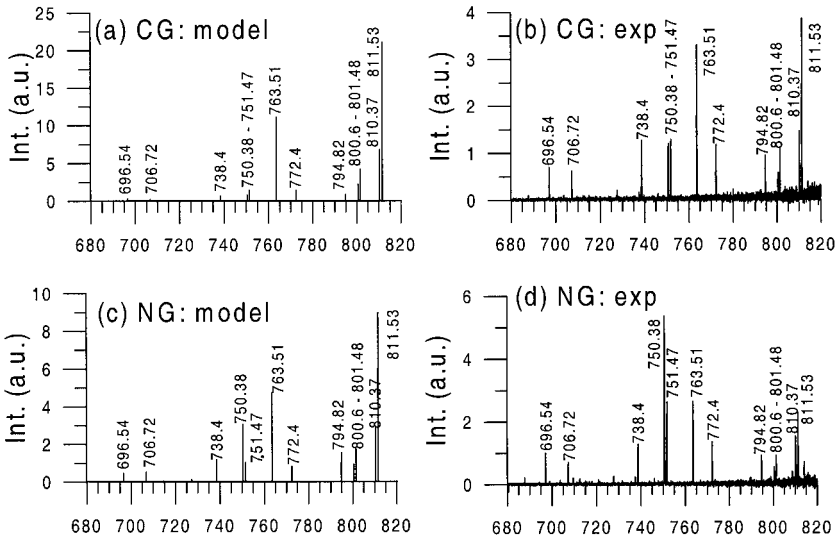

Fig. 4. Calculated and measured optical emission spectra in the 680–820 nm range, in the CG (a: model; b: experiment) and in the beginning of the NG (c: model; d: experiment), for the same conditions as in Fig. 3.

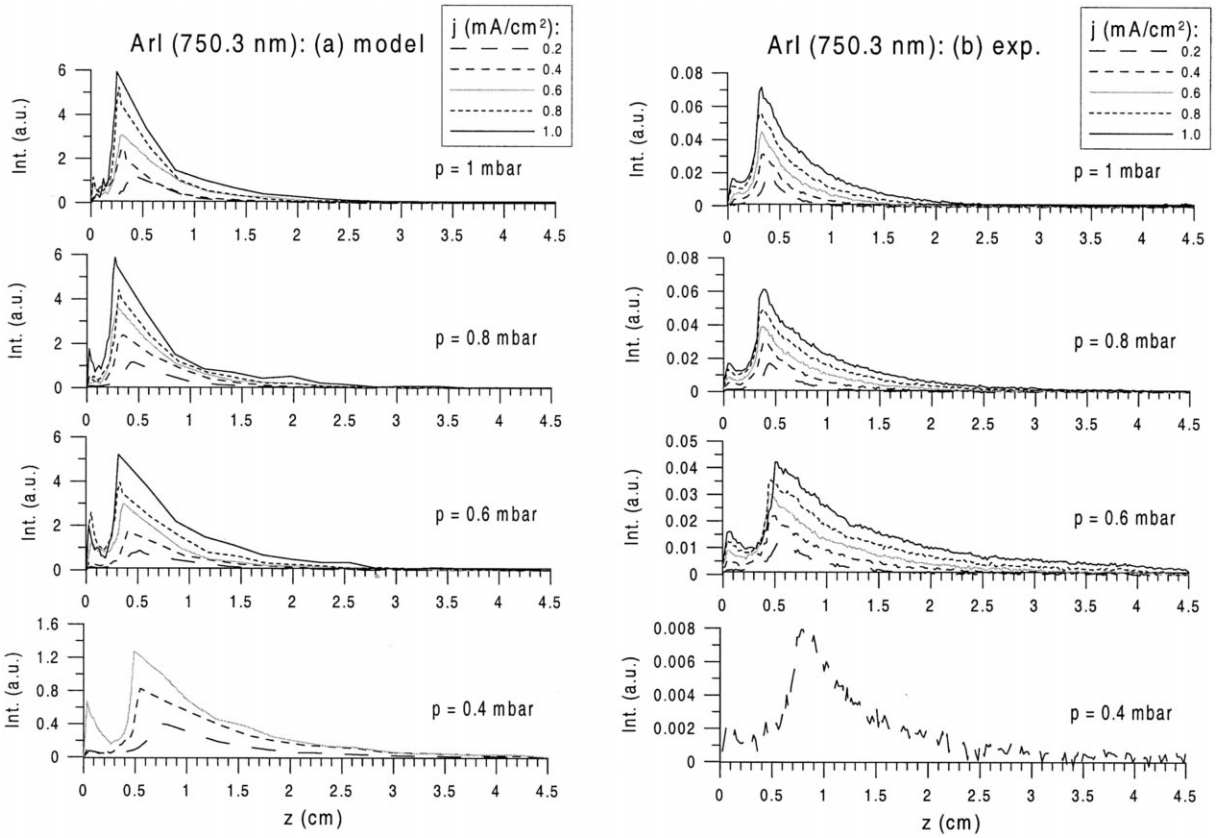

Fig. 5. Calculated (a) and measured (b) spatial distributions of the ArI 750.38 nm line, at various pressures and currents.

atom impact excitation reach their maximum at much higher energies than for electron impact excitation (see e.g. above for 811 nm emission, but this applies to all energy levels). It is easy to understand (from extrapolation from the 811 nm emission cross-section) that the higher energy levels require ion and atom impact excitation energies, which are higher than the ion and atom energies usually encountered for the discharge conditions under study. Based on cross-section data in the literature [22] for two emission lines originating from two different 4p levels, we assumed in our collisional–radiative model [3] that the cross-section for fast argon ion and atom impact excitation to the $4p[5/2]_3$ level (i.e. a lower 4p level at 13.12 eV, which emits radiation at 811.53 nm) is higher than the corresponding cross-section for excitation to the $4p'[1/2]_0$ level (at 13.48 eV, which emits the 750.38 nm line). Therefore, it is indeed expected that the first line will be more intense in the CG than the second one. In order to investigate the effect of these excitation processes, it is worth studying some specific lines in more detail as a function of axial distance from the cathode.

4.3. Spatial distributions of emission line intensities

4.3.1. The ArI 750.38 nm line

Fig. 5 illustrates the line intensities of the ArI 750.38 nm line ($4p'[1/2]_0 \rightarrow 4s'[1/2]_1$) as a function of axial position from the cathode at a range of different pressures and current densities, both calculated in the model (a) and measured experimentally (b). The currents and voltages corresponding to the current densities at the various pressures, can be deduced from Fig. 1. It appears from Fig. 5 that the intensity distribution of the 750.38 nm line is characterized by a dominant peak in the beginning of the NG, attributed to electron impact excitation. This is true for both the calculated and the experimental intensities.

A minor peak can also be observed in the CG, due to ion and atom impact excitation. This small peak increases with current at constant pressure (hence: increasing voltage), and it also increases with decreasing pressure at constant current (hence: again increasing voltage). Indeed, higher voltages mean higher ion and atom energies, and hence more ion and atom impact excitation in the CG. Moreover, lower pressures result in longer mean free paths, which means also higher ion and atom energies, and hence, more excitation. The distance of the dominant peak with respect to the cathode increases slightly with decreasing pressure, and also with decreasing current at constant pressure. Since the dominant peak is in the beginning of the NG, it means, therefore, that the length of the CDS increases with decreasing pressure and current. This is in agreement with the empirical formula proposed by Aston, which expresses the relationship between the CDS length (L_{CDS}) and the pressure (p) and current (I) in the discharge [23]:

$$L_{CDS} = \frac{A}{p} + \frac{B}{I^{1/2}}$$

where A and B are constants.

Comparing Fig. 5a,b tells us that very good agreement is reached between the calculated and the measurement intensity distributions, both with respect to the ratio of the CG and NG peaks, and to the position of the NG peak and its decay as a function of distance from the cathode. Also the effect of pressure and current on the shape of the spatial distributions and on the intensity values (i.e. increasing with current, but more or less independent of pressure, at constant current), are very similar in both experiment and model results.

4.3.2. The ArI 811.53 nm line

The spatial distributions of the ArI 811.53 nm line (originating from the lower 4p level: $4p[5/2]_3 \rightarrow 4s[3/2]_2$) are illustrated in Fig. 6a,b, for the model and experimental results, respectively, at various pressures and currents. Although the upper levels for the ArI 750.38 and 811.53 nm lines differ only by 0.36 eV (see above), the spatial distributions look quite different. Indeed, the spatial distribution for the 811.53 nm line is still characterized by a peak in the beginning of the NG, but the peak in the CG is far more intense than for the 750.38 nm line, due to the heavy

particle excitation cross-sections which appear to be higher for the 811.53 nm line compared to the 750.38 nm line.

As appears from Fig. 6a,b, the ratio of CG peak to NG peak increases with decreasing pressure (at constant current) and increasing current (at constant pressure), for the same reasons as explained above for the ArI 750.38 nm line. Indeed, a lower pressure (at constant current) and a higher current (at constant pressure) correspond both to a higher voltage, and hence to higher ion and atom energies, which give rise to more efficient ion and atom impact excitation, resulting in a higher peak in the CG. Moreover, the higher voltage yields also higher electron energies, and the latter become higher than the energy corresponding to the maximum in the excitation cross-section, hence resulting in lower electron impact excitation, and therefore a lower peak in the NG.

The agreement between calculated results (Fig. 6a) and experimental values (Fig. 6b) is again satisfactory. Indeed, good correspondence is reached for: (i) the ratio of CG/NG peaks (also as a function of voltage and current); (ii) the position of both peaks (although in the experiment, the CG peak appears to be slightly further from the cathode, and the dip between CG and NG peaks is not so pronounced as in the model, possibly due to some differences in the calculated and real length of the CDS as a function of radial distance); and (iii) the effect of pressure and current on the intensity values.

4.3.3. The ArII 476.5 nm line

We have also compared the calculated and measured spatial distributions of the ArII 476.5 nm line, as is shown in Fig. 7a,b. Since our collisional–radiative model for argon considers

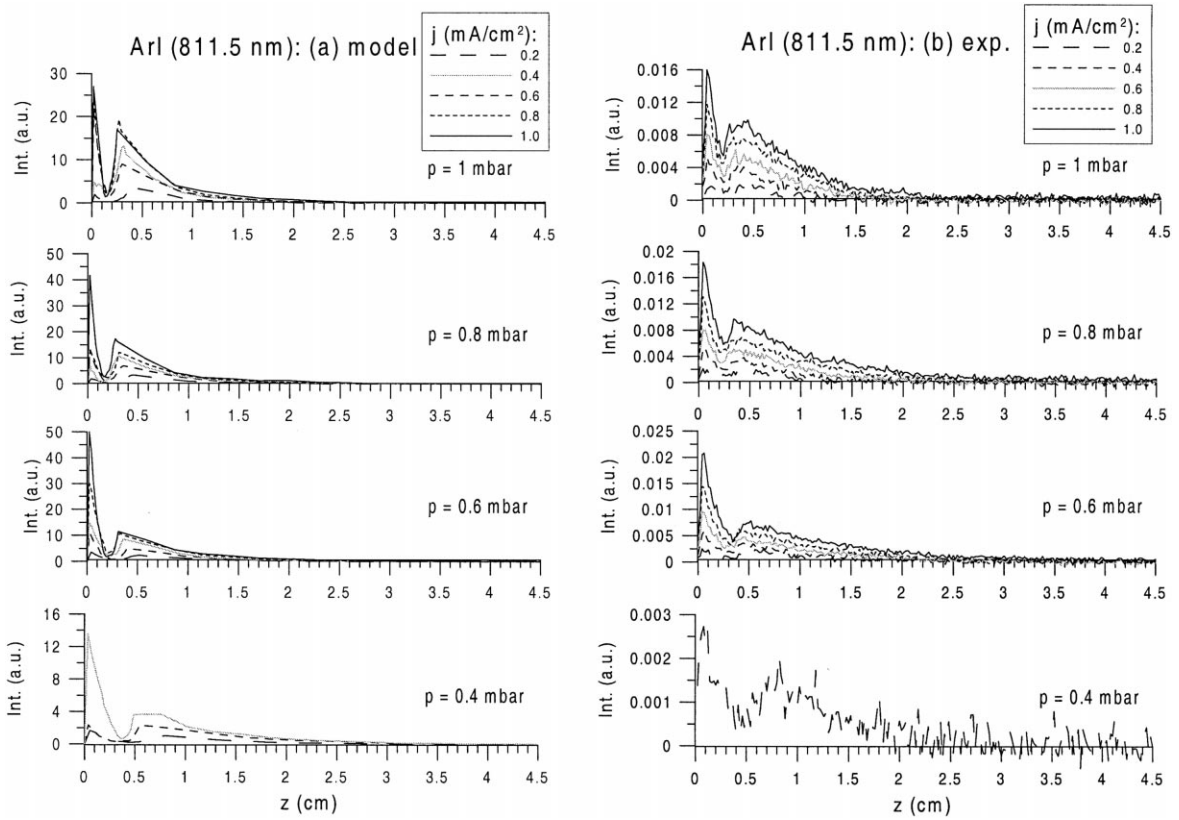

Fig. 6. Calculated (a) and measured (b) spatial distributions of the ArI 811.53 nm line, at various pressures and currents.

only argon atomic levels, the spatial distribution of this ionic line intensity is simply calculated based on the electron impact excitation rate to the upper ionic level. This ionic line is an argon ion laser line, and the upper laser level ($3p^4$ 4p $^2P_{3/2}$) is populated by direct electron impact excitation from the argon atom ground state. The cross section for this process as a function of the electron energy is adopted from Bennett et al. [24]. Fast argon ion and atom impact excitation are not considered for this line, because the energy required to excite this ionic level is expected to be much higher than the ion and atom energies at the discharge conditions under study (i.e. threshold for excitation at approx. 36 eV, but the process will only become important for much higher energies, in analogy with the know cross-sections for 811.53 nm excitation [22]). Therefore, the calculated spatial distribution of this ionic line (Fig. 7a) shows only a peak in the beginning of the NG, due to electron impact excitation. Indeed, electron impact excitation occurs mainly in the beginning of the NG, where the electrons have most suitable energy for excitation (i.e. near the energy giving rise to the maximum in the cross-section) and, even more important, where most electrons are present due to back and forth scattering in the weak electric field (see also the discussion in Bogaerts et al. [25]). The calculated spatial distribution is in good correspondence with the experimental behavior (Fig. 7b), which demonstrates that the above assumption of taking into account only electron impact excitation is justified. Comparing Fig. 7a,b tells us that not only the position and shape of the NG peak, but also the effect of pressure and current, are very similar both in the model and in the experimental results.

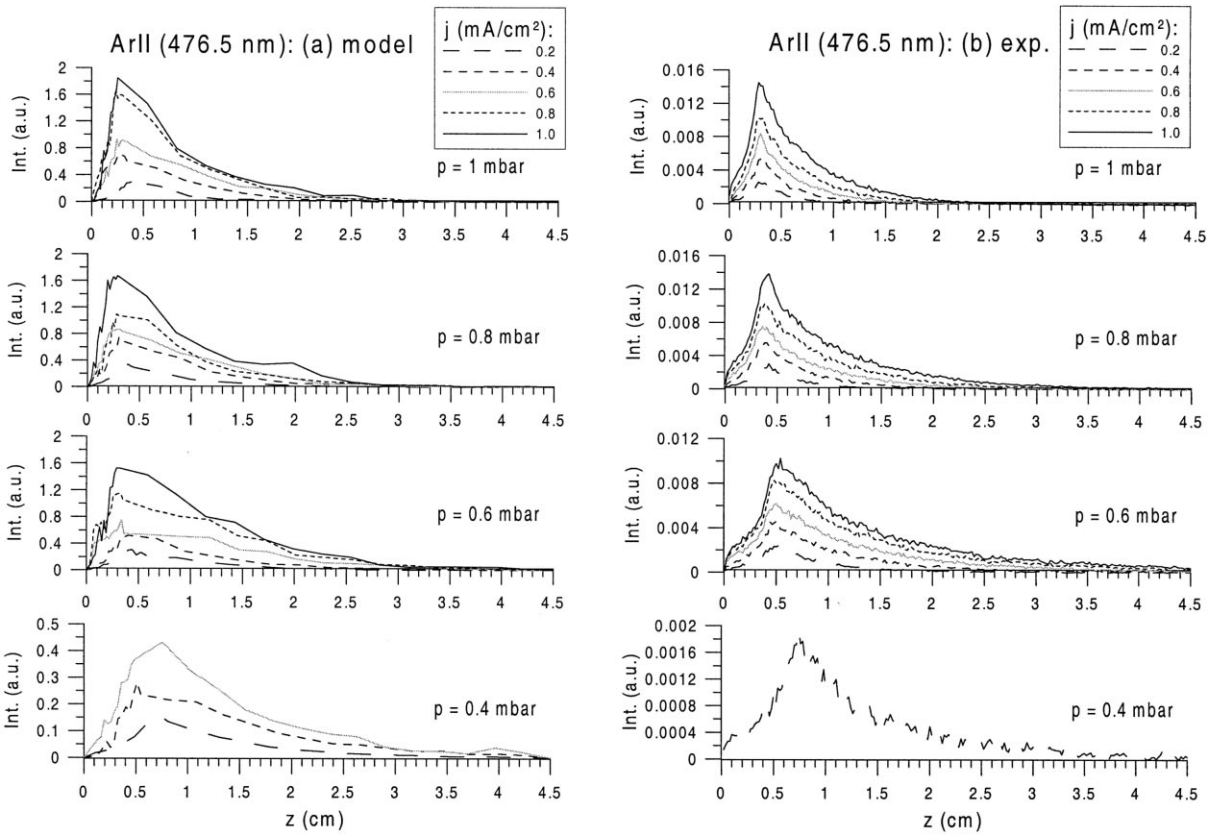

Fig. 7. Calculated (a) and measured (b) spatial distributions of the ArII 476.5 nm line, at various pressures and currents.

4.3.4. The CuI 324.75 nm line

Fig. 8a,b present the calculated and measured line intensities of the CuI 324.75 nm line, respectively, as a function of distance from the cathode, at various pressures and currents. The intensity is low in the CDS, because electron impact excitation is not so important here. It reaches a maximum at 0.3–1.0 cm from the cathode (increasing with decreasing pressure), where electron impact excitation also reaches its maximum (i.e. in the NG). Fast argon ion and atom impact excitation are not taken into account in the model for the Cu lines. This seems to be justified, since the calculated spatial profiles are in reasonable agreement with the measured results.

For a better understanding of the excitation processes of the copper atoms, the calculated copper atom ground state density profiles are illustrated in Fig. 9, at the same conditions of pressure and current as the emission lines. It appears that the Cu atom ground state density reaches a maximum at a few millimeters from the cathode, and is not characterized by a simple diffusion profile, decreasing from the sample surface. This has also been observed experimentally (e.g. [26–28]), and the explanation given in these papers was that the sputtered material might be ejected from the cathode as molecules, undetectable by atomic absorption until they become dissociated [26–28]. However, even without assuming that the sputtered material is ejected as clusters, we obtained the correct sputtered atom concentration profile with a maximum at a few millimeters from the cathode instead of at the cathode surface. The reason is that the sputtered atoms, when they leave the cathode, are first subject to collisions with the argon gas atoms until they are thermalized. It has been demon-

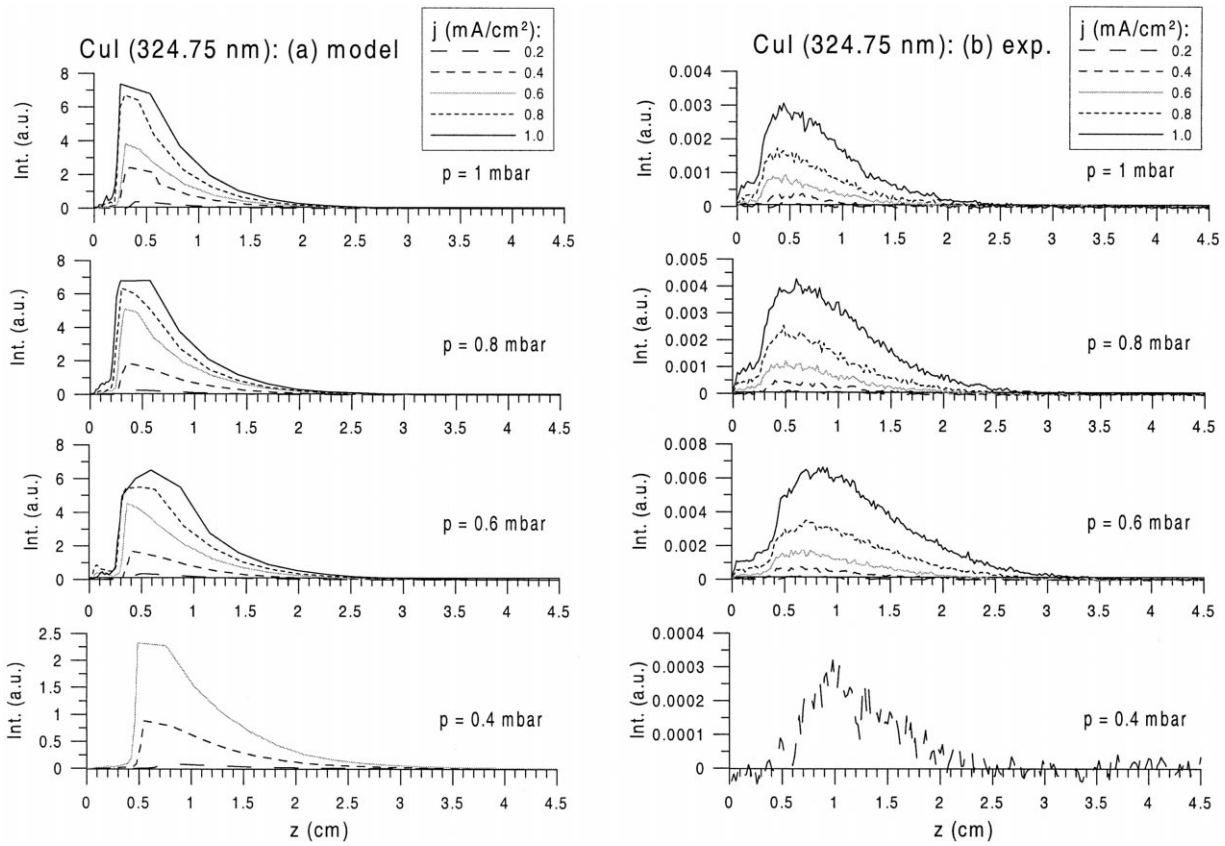

Fig. 8. Calculated (a) and measured (b) spatial distributions of the CuI 324.75 nm line, at various pressures and currents.

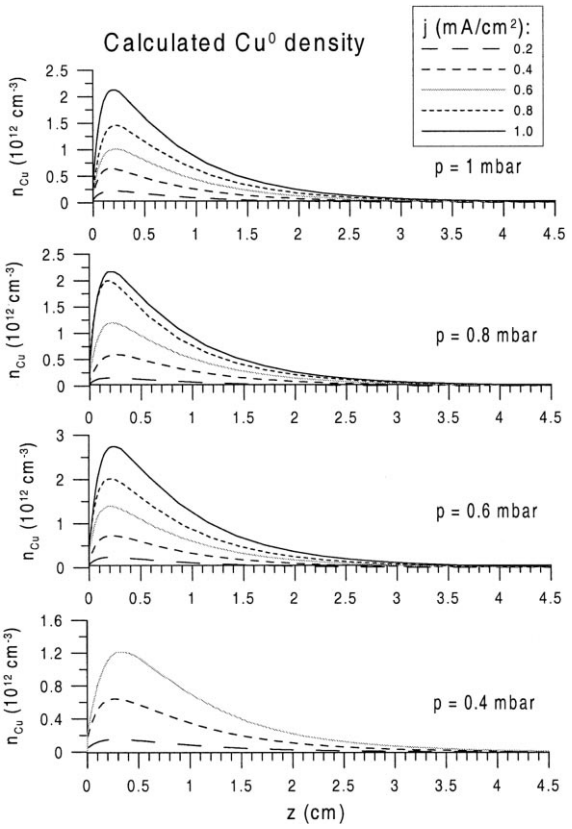

Fig. 9. Calculated spatial distributions of the copper atom ground state, at various pressures and currents.

strated that thermalization occurs on a much shorter time-scale than diffusion [29], and therefore, the so-called thermalization profile (i.e. the number of sputtered, thermalized atoms, as a function of distance from the cathode) serves as initial distribution for the further diffusion of the sputtered atoms [29–31]. Although the calculated Cu atom density profile could not be compared with experiment here, the sputtered (Ta) atom density profiles have been checked against laser-induced fluorescence and atomic absorption spectrometry measurements, and excellent agreement has been reached [32].

By comparing Figs. 8 and 9, it appears that the maximum in the Cu atom ground state density is somewhat closer to the cathode than the peak in the CuI 324.75 nm line intensities. This has two reasons: (i) the inefficient electron impact excitation in the CDS; and (ii) the phenomenon of self-absorption. Indeed, the 324.7 nm CuI line corresponds to the transition from the Cu^0 $3d^{10}$ $4p\ ^2P_{3/2}$ level to the Cu^0 $3d^{10}$ $4s\ ^2S_{1/2}$ ground state, and a fraction of the emitted radiation will be re-absorbed by the Cu atom ground state (i.e. 'radiation trapping'). This is accounted for in our model by an 'escape factor' [4]. Since the Cu atom ground state density is very high relatively close to the cathode, it will cause a considerable amount of re-absorption there, leading to a rather small amount of emitted radiation close to the cathode. Further away from the cathode, radiation trapping is not so significant anymore, due to the lower Cu atom ground state density, and the fraction of radiation escape is larger. This, together with the lack of electron impact excitation in the CDS, explains the shift in the spatial distribution of the CuI 324.75 nm line and the somewhat slower decay with distance compared to the copper atom ground state density profile.

From the comparison of Fig. 8a,b, it is clear that the model results are in close agreement to the experimental values (although the latter drop somewhat less rapidly at increasing distances), which tells us that the copper collisional–radiative model has taken into account the most important processes, and that the phenomenon of radiation trapping is more or less correctly described in the model.

4.3.5. The CuI 510.55 nm line

The spatial distributions of the CuI 510.55 nm line, resulting from the model and the measurements, are depicted in Fig. 10a,b, respectively, for a range of pressures and currents. This line originates from the same upper level as the CuI 324.75 nm line (i.e. the Cu^0 $3d^{10}$ $4p\ ^2P_{3/2}$ level), but it decays to another lower level, i.e. the Cu^0 $3d^9\ 4s^2\ ^2D_{5/2}$ level. Since the latter level has a much lower population density than the copper atom ground state, it does not give rise to re-absorption. Therefore, the calculated line intensity of the CuI 510.55 nm line drops somewhat more rapidly with increasing distance from the cathode, compared to the CuI 324.75 nm line. This might look a bit unexpected, but the reason is that radiation trapping for the 324.75 nm line is

only important close to the cathode (where the Cu atom density is high enough), so that it mainly lowers the CuI 324.75 nm line intensity at the maximum of its spatial distribution, and therefore, it makes it look broader. The CuI 510.55 nm line is not subject to self-absorption, which means that the maximum in the spatial distribution is not lowered, and that it seems to drop somewhat more rapidly as a function of distance from the cathode.

The calculated spatial distributions are in reasonable agreement with the experimental data for the CuI 510.55 nm line, presented in Fig. 10b. It appears from Fig. 10a,b that the calculated line intensities drop again somewhat more rapidly than experimentally observed, which might be explained by a somewhat too low copper diffusion coefficient in the model. Indeed, a higher diffusion coefficient generally yields a broader copper density profile, and hence, a broader spatial distribution of the optical emission intensities. Nevertheless, the agreement between the model and experiment in Fig. 10a,b is quite satisfactory, also with respect to the effect of pressure and current.

5. Conclusion

Optical emission intensities of argon and copper lines have been calculated for a d.c. argon glow discharge with copper cathode. Special attention has been paid to the spatial distributions of some selected lines as a function of pressure and current. The calculated line intensities have been compared with measured values, and in general good agreement has been reached, at least qualitatively, indicating that the model takes

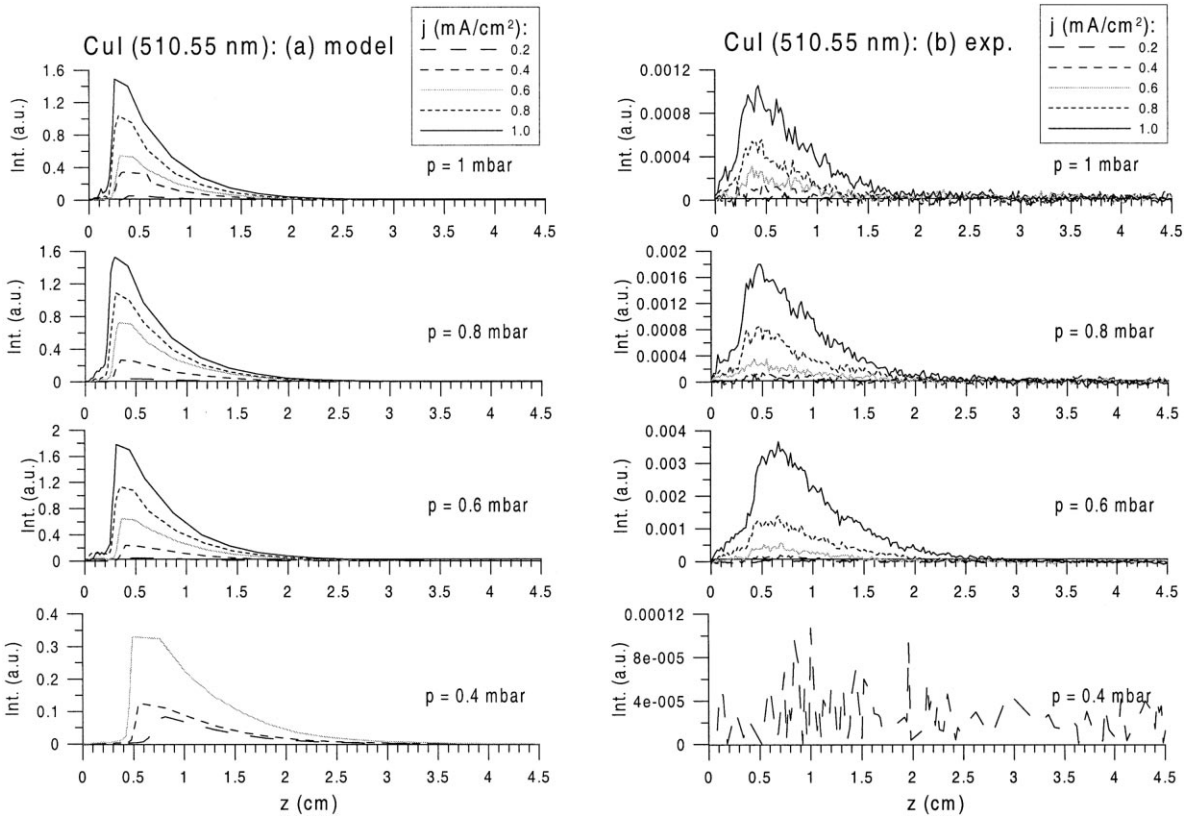

Fig. 10. Calculated (a) and measured (b) spatial distributions of the CuI 510.55 nm line, at various pressures and currents.

into account the correct excitation processes and uses reasonable cross-sections.

For the intensity distribution of the argon atomic lines, it was found that lines originating from levels belonging to the lower 4p configuration exhibit a strong peak in the CG and a smaller peak in the beginning of the NG, whereas lines originating from higher 4p levels are characterized by a dominant peak in the beginning of the NG and only a minor peak in the CG. The argon ionic line was only characterized by a NG peak. This demonstrates that the argon atom lower 4p levels (as well as the 4s levels) can be excited by both electron and fast argon atom and ion impact excitation, whereas the higher 4p levels (as well as all higher atomic levels and the ionic levels) are predominantly (or exclusively) populated by electron impact excitation. The CuI lines were found to exhibit a maximum intensity in the NG, attributed to electron impact excitation from the Cu atom ground state. The spatial distribution of the CuI 324.75 nm line is somewhat broader than that of the CuI 510.55 nm line. The reason is that the 324.75 nm line is a resonant line to the copper atom ground state, which is strongly subject to self-absorption ('radiation trapping'), at least at the maximum of its spatial distribution. This results in a lowering of the maximum intensity, and hence, it looks like a broadening in the spatial distribution.

It is demonstrated in this paper that from the comparison of calculated and experimental optical emission intensities, interesting information can be obtained about the role of various excitation processes. In future work, we would like to investigate the effect of decreasing discharge tube diameter, because the experiment [10] revealed the possible formation of a positive column-like or anode fall-like region, and a good understanding of these experimental observations [10] necessitates detailed numerical modeling.

Finally, it should be mentioned that, although the results are not presented here in a typical analytical glow discharge source, but in a source equipped with the necessary diagnostics, the discharge conditions and cell dimensions are more or less comparable to analytical glow discharges. From our previous calculations, we know that the presently obtained results (i.e. occurrence and positions of the peaks in the spatial distributions of the different lines) can be generalized to analytical glow discharge sources, such as the Grimm-type source, as long as the discharges consist of a CDS and a NG, which is generally the case for analytical glow discharges.

Acknowledgements

A. Bogaerts is indebted to the Flemish Fund for Scientific Research (FWO) for financial support. This research is also sponsored by a NATO SfP Project (SfP 971989), OTKA-T-25989, P6/97 Hungarian-Portugal Bilateral Project and by the Federal Services for Scientific, Technical and Cultural Affairs (DWTC/SSTC) of the Belgian Prime Minister's Office through IUAP-IV (Conv. P4/10). Finally, the authors wish to thank K. Rozsa and L. Szalai for useful discussions, and T.J. Forgacs, J. Toth, E. Sarkozi and Gy. Csaszar for the construction of the discharge tube.

References

[1] R.K. Marcus, Glow Discharge Spectroscopies, Plenum, New York, 1993.
[2] R. Payling, A. Bengtson, D. Jones, Glow Discharge Optical Emission Spectrometry, Wiley, Chichester, 1996.
[3] A. Bogaerts, R. Gijbels, J. Vlcek, J. Appl. Phys. 84 (1998) 121–136.
[4] A. Bogaerts, R. Gijbels, R.J. Carman, Spectrochim. Acta Part B 53 (1998) 1679–1703.
[5] A. Bogaerts, R. Gijbels, J. Vlcek, Spectrochim. Acta Part B 53 (1998) 1517–1526.
[6] A. Bogaerts, R. Gijbels, J. Anal. At. Spectrom. 13 (1998) 721–726.
[7] A.V. Phelps, B.M. Jelenkovic, Phys. Rev. A 38 (1988) 2975–2990.
[8] D.A. Scott, A.V. Phelps, Phys. Rev. A 43 (1991) 3043–3056.
[9] K. Rozsa, A. Gallagher, Z. Donko, Phys. Rev. E 52 (1995) 913–918.
[10] Z. Donko, G. Bano, L. Szalai, K. Kutasi, K. Rozsa, M. Pinheiro, N. Pinhao, J. Phys. D: Appl. Phys. 32 (1999) 2416–2425.
[11] Z.M. Jelenak, Z.B. Velikic, J.V. Bozin, Z.Lj. Petrovic, B.M. Jelenkovic, Phys. Rev. E 47 (1993) 3566–3573.
[12] S.B. Radovanov, B. Tomcik, Z.Lj. Petrovic, B.M. Jelenkovic, J. Appl. Phys. 67 (1989) 97–107.

[13] F. Guimaraes, J.B. Almeida, J. Bretagne, Plasma Sources Sci. Technol. 2 (1993) 138–144.
[14] Z.Lj. Petrovic, S. Bzenic, J. Jovanovic, S. Djurovic, J. Phys. D: Appl. Phys. 28 (1995) 2287–2293.
[15] Z.Lj. Petrovic, V.D. Stojanovic, J. Vac. Sci. Technol. A 16 (1998) 329–336.
[16] F. Guimaraes, J. Bretagne, Plasma Sources Sci. Technol. 2 (1993) 127–137.
[17] A. Bogaerts, Plasma Sources Sci. Technol. 8 (1999) 210–229.
[18] N. Pinhao, J. Phys. D: Appl. Phys. 27 (1994) 1184–1192.
[19] A. Bogaerts, R. Gijbels, V.V. Serikov, J. Appl. Phys. 87 (2000) 8334–8343.
[20] E.B.M. Steers, R.J. Fielding, J. Anal. At. Spectrom. 2 (1987) 239–244.
[21] E. Eggarter, J. Chem. Phys. 62 (1975) 833–847.
[22] A.V. Phelps, J. Phys. Chem. Ref. Data 20 (1991) 557–573.
[23] F.W. Aston, Proc. R. Soc. London Ser. A 79 (1907) 80–85.
[24] W.R. Bennett Jr., G.N. Mercer, P.J. Kindlmann, B. Wexler, H. Hyman, Phys. Rev. Lett. 17 (1966) 987–991.
[25] A. Bogaerts, R. Gijbels, W.J. Goedheer, J. Appl. Phys. 78 (1995) 2233–2241.
[26] A.J. Stirling, W.D. Westwood, J. Phys. D: Appl. Phys. 4 (1971) 246–252.
[27] N.P. Ferreira, H.G.C. Human, Spectrochim. Acta Part B 36 (1981) 215–229.
[28] K. Hoppstock, W.W. Harrison, Anal. Chem. 67 (1995) 3167–3171.
[29] J.A. Valles-Abarca, A. Gras-Marti, J. Appl. Phys. 55 (1984) 1370–1378.
[30] M. van Straaten, R. Gijbels, A. Vertes, Anal. Chem. 64 (1992) 1855–1863.
[31] A. Bogaerts, R. Gijbels, J. Appl. Phys. 79 (1996) 1279–1286.
[32] A. Bogaerts, E. Wagner, B.W. Smith, J.D. Winefordner, D. Pollmann, W.W. Harrison, R. Gijbels, Spectrochim. Acta Part B 52 (1997) 205–218.